Preliminary Computational Study of Transition on a Flared Cone Using Random Forcing

Andrew Shuck*, Jonathan Poggie†, and Gregory Blaisdell‡
Purdue University, West Lafayette, IN 47906-2045, USA

This study presents the preliminary analysis of a high speed boundary layer on a flared cone using Linear Stability Theory and Direct Numerical Simulation. In flight or wind tunnels, noise propagates into the boundary layer from the atmospheric turbulence or the noise generated from turbulent sidewall boundary layers. Linear Stability Theory can predict the frequency that is most likely going to be amplified. However, it cannot predict the nonlinear regime, that is, how the flow will breakdown to turbulence. In order to track the disturbances all the way to breakdown, one must use DNS. By introducing random forcing into the freestream of a Direct Numerical Simulation, a more natural process of amplification and transition can be observed as disturbances enter, travel, and grow in the boundary layer.

I. Introduction

As flight speed goes up, heat transfer to the surface of the vehicle becomes increasingly important. The heating is increased when the boundary layer transitions from laminar to turbulent. Studying transition is difficult because the process is highly nonlinear and depends on many factors. This requires the use of Linear Stability Theory (LST) or the use of computationally expensive Direct Numerical Simulations (DNS) to gain insight. The present study uses the Flared Cone geometry, detailed in Ref. [1], that was tested in the Boeing/AFOSR Mach 6 Quiet Tunnel (BAM6QT). Quiet tunnels have disturbance levels that are exceptionally low and the BAM6QT has freestream pressure fluctuations lower than "0.02% of the mean" [2]. Chynoweth's [1] measurements show that there is an unstable second mode frequency of around 300 kHz which causes natural transition. Additionally, the second mode causes "primary streaks and secondary streaks" in the heat transfer distribution along the surface of the cone as the boundary layer transitions.

Hader and Fasel [3] simulate the flared cone and observe transition by putting random forcing waves in the highly resolved boundary layer. The grid resolution involves an azimuthal resolution of around 29 points per degree of the cone. By doing this, they are able to achieve transition and observe the primary and secondary streaks as found in Chynoweth's experiments [1]. This present study used a two-stage DNS calculation and introduce the disturbances in the freestream around the cone instead of in the boundary layer. This approach may lead to a more realistic representation of the effects of freestream noise on the boundary layer. The first stage is to calculate a basic state of the whole flared cone geometry and extract a flow profile to use as an input for the DNS. The second stage is to use this extract to calculate on a partial, but much more resolved grid. The Langley Stability and Transition Code (LASTRAC) was used to confirm the unstable frequencies involved in transition.

II. Methodology

The freestream conditions are modeled on Run 1611 reported by Chynoweth [1]. The wall is considered isothermal because of the very short run time of the BAM6QT. These conditions are shown in Table 1. The geometry is a flared cone created from a circle with a radius of 3 meters and is shown in Fig. 1a. It has a nose tip of radius 0.0001m and body length of 0.51m. The scale of the nose tip compared to the body length provides some challenges in computing the flow. More specifically, the minimum cell edge length significantly affects the computational requirements and is limited by the azimuthal resolution and the radius of the nose tip. In order to achieve a resolution similar to Hader [3] and maintain a reasonable minimum edge length, a basic state is calculated, and an inflow profile is extracted and imposed on a portion of the cone in a DNS computation. Two grids and two solvers are used to ensure the correct inflow is provided

*Graduate Student, School of Aeronautics and Astronautics, AIAA Student Member
†Professor, School of Aeronautics and Astronautics, AIAA Associate Fellow
‡Professor, School of Aeronautics and Astronautics, AIAA Associate Fellow

Approved for public release: distribution unlimited
Case Number: AFRL-2020-0416

Table 1 Freestream Conditions

Mach	6
Freestream Velocity	863 m/s
Freestream Pressure	684 Pa
Freestream Temperature	51.46 K
Unit Reynolds Number	12E6 /m
Isothermal Surface Temp.	300 K

to the DNS. The first set of calculations involve a mesh with a nose tip that is numerically sharp with 1E-5m Δy across the entire surface of the cone. A lower resolution base mesh for both nose tip types is shown for clarity in Fig. 1b. The numerically sharp nose tip is shown in Fig. 2a and is computed using the CREATE-AV Kestrel code and the high-order Purdue University code Wabash. A second set of calculations involve a mesh that is unstructured and models the nose tip of the cone. This is done by applying an O-grid to the tip and combining the nose tip block and the body block with a few non-hexahedral cells. Calculations for this mesh were carried out using Kestrel. The mesh is shown in Fig. 2b. The base grid (the part of the grid downstream of the nose region) does not change so it is not shown again. The DNS grid has 9025x600x151 grid points in the streamwise, wall normal, and azimuthal directions, respectively. It is a cone section of 5 degrees with the nose tip cut off at a location of X = 0.05m. An outline of the mesh is shown in Fig. 3. This setup allows the minimum edge length to be held at 1E-6m, maintaining a similar azimuthal resolution to Hader [3].

Wabash is used in this study and is detailed in Ref. [4],[5],[6]. It is an in-house, high-order, structured, overset CFD code developed by J. Poggie at Purdue University. The simulation proceeds in steps of low-order and then high-order. It starts off with explicit second-order differencing and first-order implicit time stepping in order to promote numerical stability as a preliminary solution is found. Once this is done, the code is switched to implicit sixth-order differencing with explicit fourth-order Runge-Kutta time stepping and progressed until it has converged. From here, the basic state and inflow profile are extracted and put into LASTRAC and the DNS. When running the DNS, random forcing waves will be applied to a high-order simulation after the basic state laminar solution has converged.

Kestrel is an unstructured, high fidelity solver optimized to obtain solutions for many types of fixed-wing aircraft. More details about the development and capabilities of Kestrel are found in Ref. [7],[8]. The flow was calculated as laminar using 2nd order space, 2nd order time with 2nd order sub-iterations, inviscid HLLE++, and viscous LDD+ flux schemes. A local time stepping scheme was used to accelerate to a steady state and handle the nose tip and body scale difference. Once the solution converges, an inflow profile can be extracted and applied to a DNS inflow condition.

The DNS is computed in a similar manner to the Wabash basic state solution mentioned above. Once the high-order solution is found, random forcing waves are introduced into the DNS. The method of forcing is similar to that employed by Tufts et al. [9] and by Andrews and Poggie [10]. The random wave forcing was constructed to be fully resolved numerically and are continuous across boundaries under domain decomposition. The forcing waves are placed in the freestream allowing the disturbances to propagate through the shock layer and into the boundary layer. An example of this forcing region is shown in Fig. 4, and is created by choosing a starting location, ending location, height, and angle. The waves are generated in a conical frustum shape around the entire cone. The frequency of the waves can be uniformly defined on a certain range, or set to an approximation of a wind tunnel that has experimental freestream noise spectra. Currently approximations of the BAM6QT and the AEDC-VKF Tunnel B have been incorporated into the code.

The approximation of the freestream noise profile of the BAM6QT use data from Gray et al. [11] when the tunnel is not in operation, when it is in quiet operation, and when it is in noisy operation. The three profiles are seen in Fig. 5. Each profile is fit with either a power law fit or a polynomial fit. Initially, the noisy flow is approximated with a power law fit, the quiet flow is approximated with a 12-degree polynomial, and the no flow data is fit with a 6-degree polynomial. These approximations can be seen in Fig. 6. The no flow noise approximation was subtracted from the other flows to eliminate the sensor noise. Finally, the noisy and quiet flows are refit to reduce the order of the equations. The noisy flow stays as a power law fit and the quiet flow is reduced to a 4-degree polynomial. The updated approximations are the available BAM6QT noise options in Wabash and are shown in Fig. 7. Additionally, the approximation of the noise profile in the AEDC-VKF Tunnel B is detailed by Andrews and Poggie [10].

LASTRAC is used to supplement the results of the spectral analysis carried out on the DNS calculation. It is an LST tool used to determine frequencies and their N-Factor to see if a disturbance will reach the nonlinear regime of amplification. It takes a structured, axisymmetric slice of the results and applies disturbances to each station along the

cone. This means a structured slice of the numerical tip solution from Wabash is used. In this case, it will calculate the growth factors of frequencies ranging from 70 kHz to 1000 kHz. A second mode instability is the main cause of transition for this cone, so an unstable frequency characteristic of the second mode is expected.

III. Results

The three initial basic state solutions are the modeled tip in Kestrel, and the numerical tip in Wabash and Kestrel. The skin friction coefficient magnitude is shown for the three different solutions in Fig. 8. The numerical tip cases using Wabash and Kestrel employ the same grid, but differing solvers. One can see similarities in each of the solutions, but there are some differences. The modeled tip solution found slightly higher skin friction than the numerical tip solutions. If the contour range of skin friction is narrowed, then four streamwise streaks can be found on all cases. The differences in the magnitude are not very large and are shown in Fig. 9. In order to more easily identify the differences, three different surface profiles were extracted and compared. The extraction locations are seen in Fig. 10. Two streamwise profiles are extracted down the center of a streak and halfway between two streaks at approximately 45 degrees. The last extracted profile is a circumferential curve at X = 0.4m. These results are seen in Fig. 11. The most interesting result is from the circumferential profile in Fig. 11d where four distinct streaks appear at 90 degree intervals. The magnitude of these streaks are within 3% of the average value. It is suspected that these are stationary instabilities associated with streamline curvature, as mentioned by Porter and Poggie[12]. Multiple calculations involving different grid decompositions and solver settings were carried out, but are not shown because the results were identical.

A LASTRAC calculation is carried out on a 2D "on streak" slice of the numerical tip solution found in Wabash. It is currently unknown if azimuthal location of the slice affects the LASTRAC calculation in regard to the streamwise streaks. In order to have an idea of where the nose tip can be cut off for the DNS Inflow condition, it is important to determine when the frequencies begin to amplify. According to the measurements of Chynoweth [1], the unstable frequencies are around 300 kHz, and frequencies from 70 kHz to 1000 kHz are tested in LASTRAC. The resulting N-Factors are shown in Fig. 12. The most unstable frequency of around 290 kHz is found in LASTRAC, which is very close to the experimental findings. Additionally, it is shown that any distance before X = 0.1m can be used as the inflow position because the instability waves do not grow before that station. The distance of X=0.05m was used to maintain as much of the cone as possible while keeping the minimum circumferential cell edge length at 1E-6m. More detail about the inflow position and extract is available in Fig. 13. The profiles in Fig. 13a, 13b are extracted at X=0.05m and used as the inflow condition for the DNS grid. The profiles are extracted "on streak", but the magnitude of the streamwise streaks at this station are within 0.01% of the average azimuthal value. The DNS is ongoing and is not presented.

IV. Conclusion

The DNS is currently running to solve the base state with the provided inflow profile. Multiple time stepping schemes are being tested to determine which one provides the largest timestep with the most stability. Once this is computed, freestream noise will be applied, and the growth of any unstable frequencies will be analyzed. Finally, further analysis will be done on the heat transfer of the cone to identify if any primary and secondary streaks appear as they did in Chynoweth [1] and Hader [3].

Acknowledgments

The present work was supported by the AFRL. Computational resources were provided by the AFRL DSRC and ERDC DSRC. This paper was cleared for public release: distribution unlimited, with the case number AFRL-2020-0416.

References

[1] Chynoweth, B. C., *Measurements of Transition Dominated by the Second-Mode Instability at Mach 6*, Ph.D. Dissertation, Purdue University School of Aeronautics and Astronautics, May 2018.

[2] Steen, L. E., *Characterization and Development of Nozzles for a Hypersonic Quiet Tunnel*, Master's Thesis, Purdue University School of Aeronautics and Astronautics, December 2010.

[3] Hader, C., and Fasel, H., "Towards simulating natural transition in hypersonic boundary layers via random inflow disturbances," *Journal of Fluid Mechanics*, Vol. 847, 2018, p. R3.

[4] Poggie, J., Bisek, N. J., and Gosse, R., "Resolution effects in compressible, turbulent boundary layer simulations," *Computers and Fluids*, Vol. 120, 2015, pp. 57–69. https://doi.org/10.1016/j.compfluid.2015.07.015.

[5] Porter, K. M., and Poggie, J., "Selective Upstream Influence on the Unsteadiness of a Separated Turbulent Compression Ramp Flow," *Physics of Fluids*, Vol. 31, 2019, p. 016104. https://doi.org/10.1063/1.5078938.

[6] Poggie, J., and Porter, K. M., "Flow structure and unsteadiness in a highly confined shock-wave–boundary-layer interaction," *Physical Review Fluids*, Vol. 4, 2019, p. 024602. https://doi.org/10.1103/PhysRevFluids.4.024602.

[7] McDaniel, D. R., and Tuckey, T. R., "HPCMP CREATE^{TM}-AV Kestrel New and Emerging Capabilities," *AIAA Paper 2020-1525*, January 2020. https://doi.org/10.2514/6.2020-1525.

[8] McDaniel, D. R., and Morton, S. A., "HPCMP CREATE^{TM}-AV Kestrel Architecture, Capabilities, and Future Directions," *AIAA Paper 2018-0025*, January 2018. https://doi.org/10.2514/6.2018-0025.

[9] Tufts, M. W., Bisek, N. J., and Kimmel, R. L., "Implicit Large-Eddy Simulation of Discrete Roughness Boundary-Layer Transition with Added Perturbations," *AIAA Paper 2019-2967*, June 2019. https://doi.org/10.2514/6.2019-2967.

[10] Andrews, G. M., and Poggie, J., "Effects of Freestream Acoustic Disturbances on Hypersonic Boundary Layer Stability," *AIAA Paper 2020-2995*, June 2020. https://doi.org/10.2514/6.2020-2995.

[11] Gray, K. A., Chynoweth, B. C., Edelman, J. B., McKiernan, G. R., Wason, M. P., and Schneider, S., "Boundary-Layer Transition Measurements in the Boeing/AFOSR Mach-6 Quiet Tunnel," *AIAA Paper 2017-0068*, January 2017. https://doi.org/10.2514/6.2017-0068.

[12] Porter, K. M., and Poggie, J., "Laminar and Turbulent Flow Calculations for the HIFiRE-5b Flight Test," *AIAA Paper 2017-3132*, June 2017. https://doi.org/10.2514/6.2017-3132.

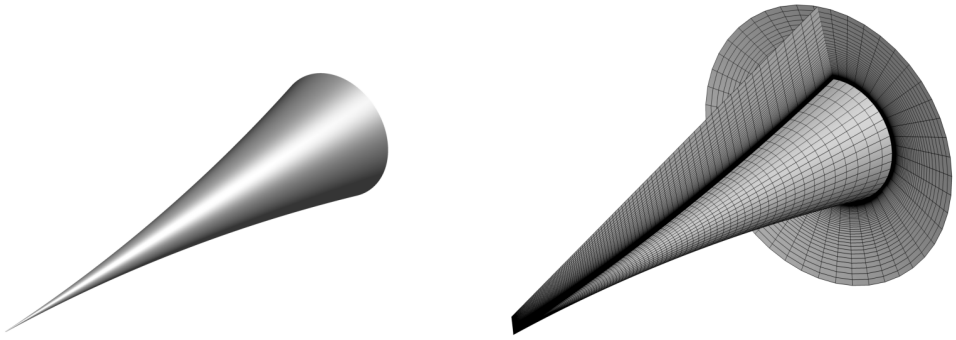

(a) Geometry **(b) Base Mesh**

Fig. 1 Flared Cone

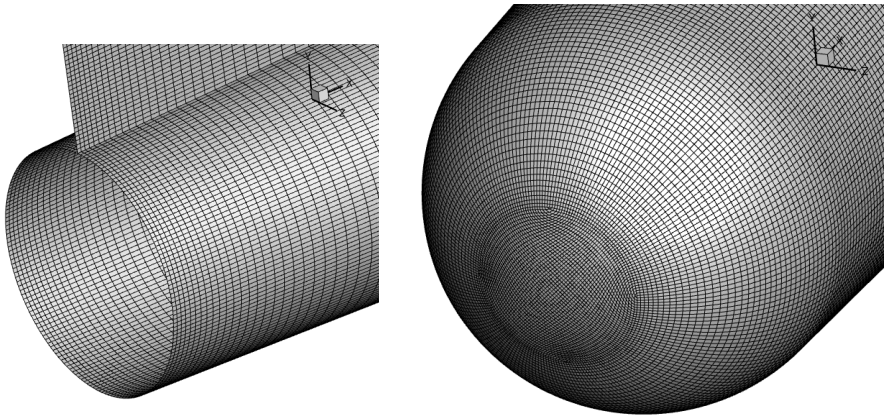

(a) Numerically Sharp Nose Tip (b) Modeled Nose Tip

Fig. 2 Nose Tip Details

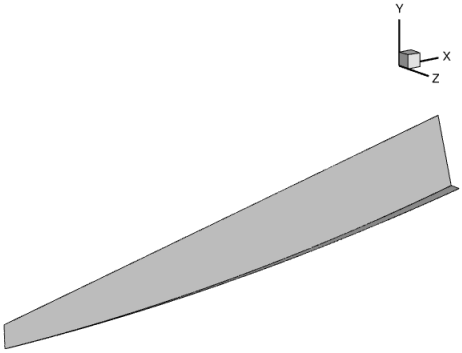

Fig. 3 DNS Computational Domain

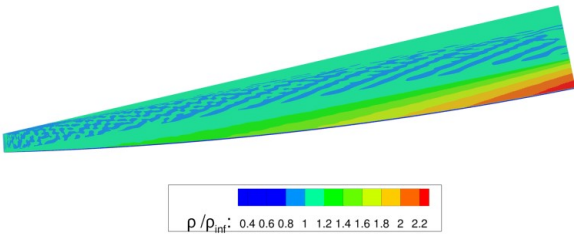

Fig. 4 Sample Forcing Region

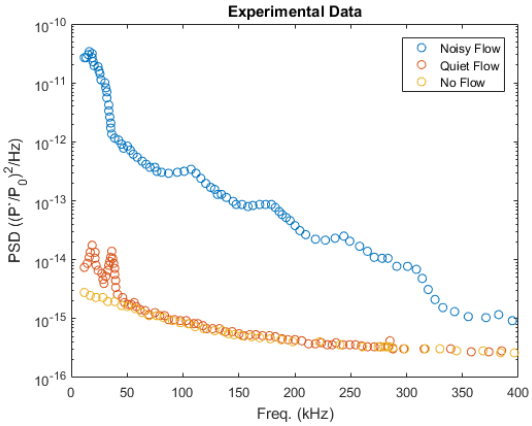

Fig. 5 BAM6QT Freestream Noise Profiles

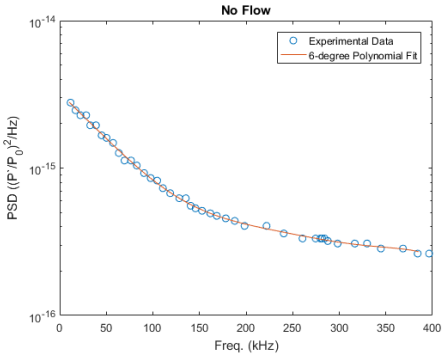

(a) No Flow Fit

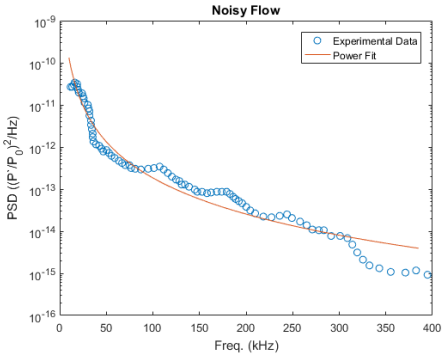

(b) Noisy Flow Fit

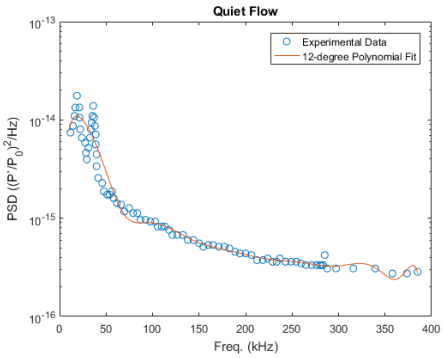

(c) Quiet Flow Fit

Fig. 6 Data Fitting

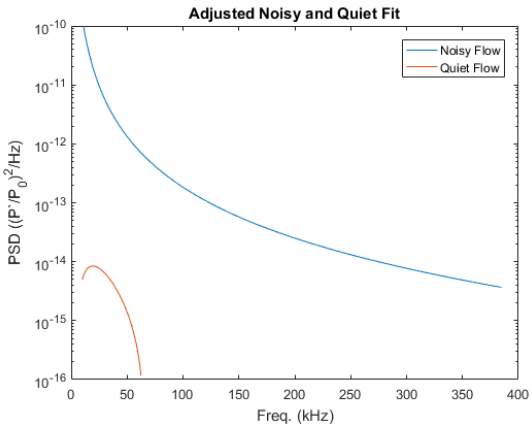

Fig. 7 Noise Approximation for Noisy and Quiet Flow

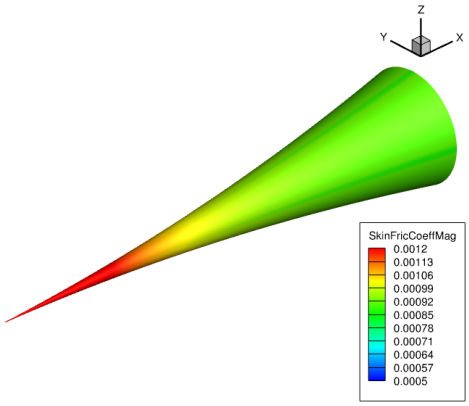

(a) Numerically Sharp Tip: Wabash

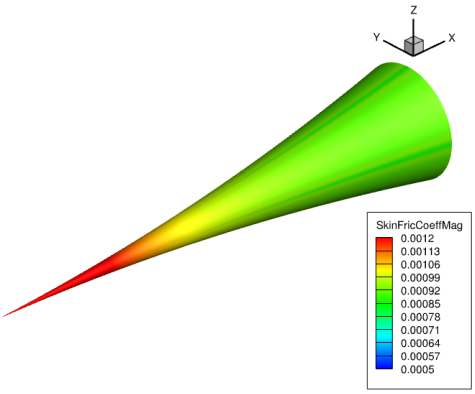

(b) Numerically Sharp Tip: Kestrel

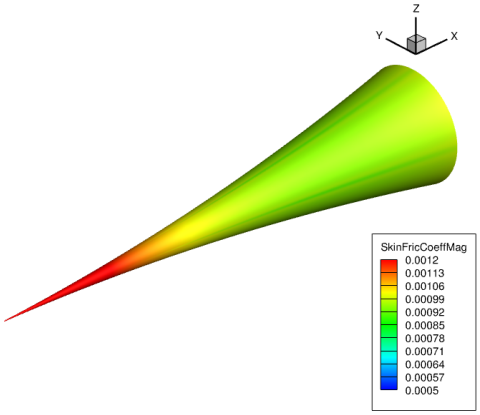

(c) Modeled Tip: Kestrel

Fig. 8 Skin Friction Coefficient Magnitude

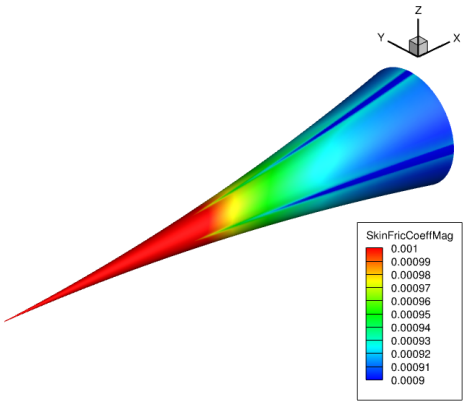

(a) Numerically Sharp Tip: Wabash

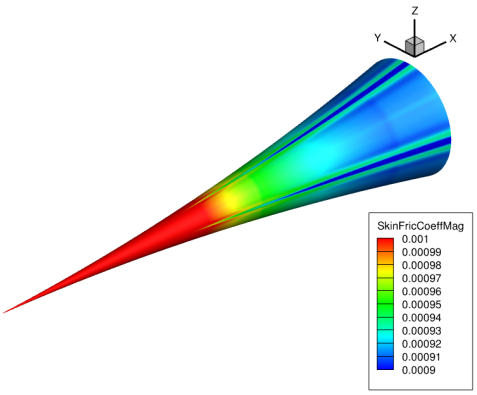

(b) Numerically Sharp Tip: Kestrel

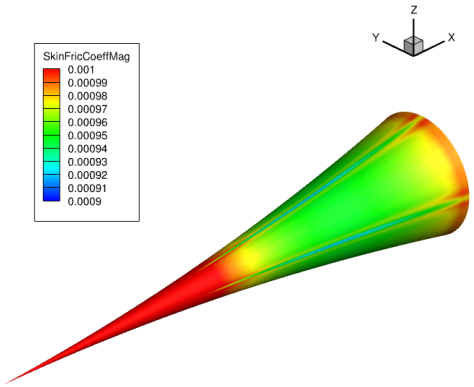

(c) Modeled Tip: Kestrel

Fig. 9 Closer look: Skin Friction Coeff. Mag.

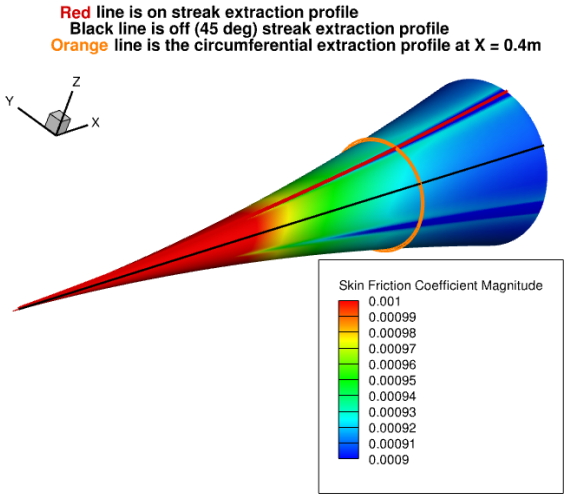

Fig. 10 Extraction Locations

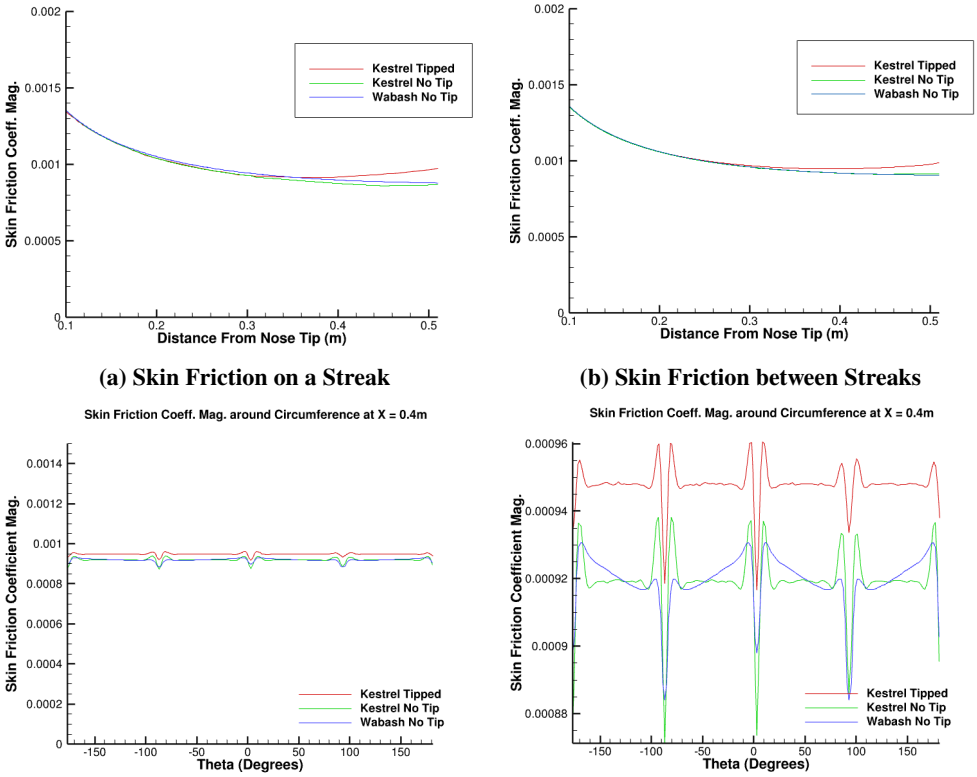

(a) Skin Friction on a Streak

(b) Skin Friction between Streaks

(c) Circumferential Skin Friction

(d) Closer: Circumferential Skin Friction

Fig. 11 Skin Friction Coeff. Mag. Profiles

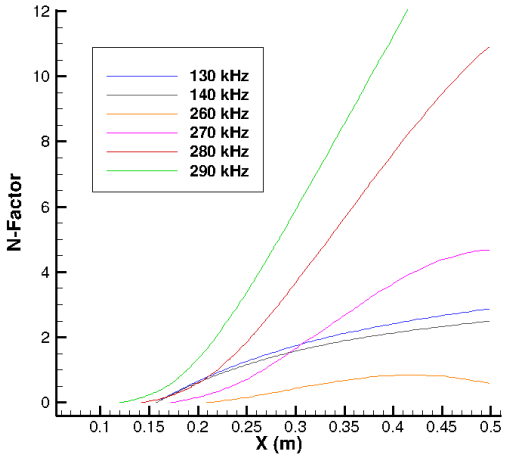

Fig. 12 LASTRAC Results

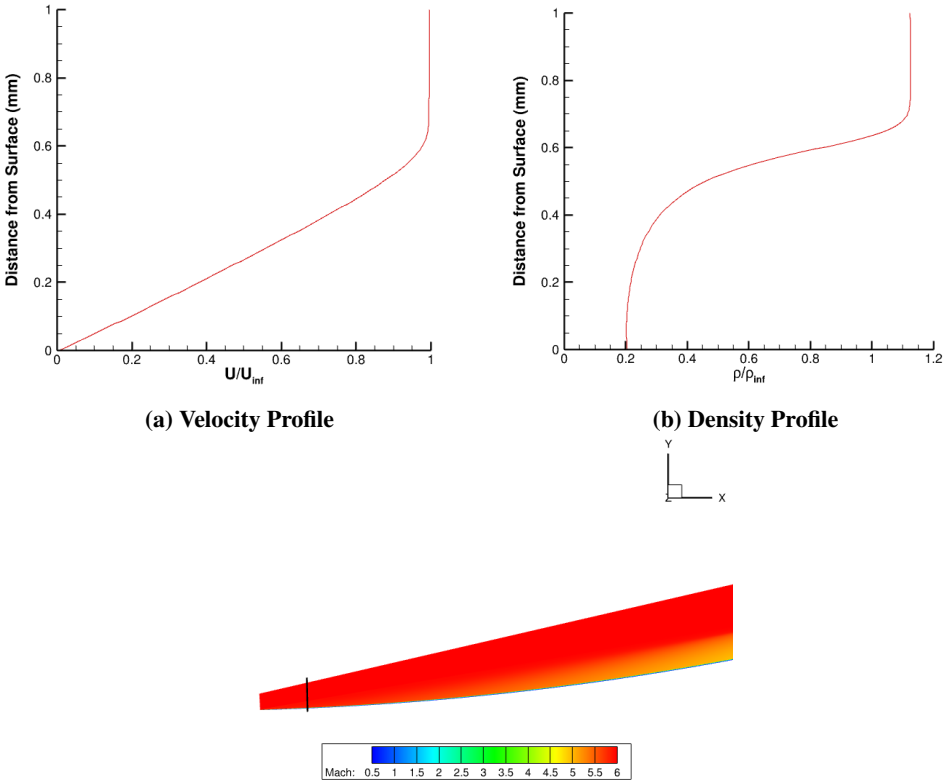

(a) Velocity Profile

(b) Density Profile

(c) Extract Location (Black Line)

Fig. 13 Inflow Extract Details